A Geochemical and Petrographic Analysis of the Basalts of the Ricardo Formation, Southern El Paso Mountains, CA

By
Cami Jo Anderson
Geological Sciences Dept.
California State Polytechnic University
Pomona, CA

Senior Thesis
Submitted in partial fulfillment
of requirements for the
B.S. Geology Degree

TABLE OF CONTENTS

ABSTRACT

The Miocene Ricardo Group of the southern El Paso Mountains consists of lucustrine sedimentary rocks interlayered with felsic tuffs and basalt flows. The basalts were sampled and analyzed geochemically and petrographically. The results of those analyses were compared to data from other Mojave/Owens Valley basalt fields. Major elements show dramatic differences. Ricardo volcanics have significantly lower alkali (Na_2O + K_2O) content, plotting as tholeiites on a basalt tetrahedron. This is in marked contrast to the distinctly alkaline character of other fields. CIPW analyses support the geochemical data. Ricardo basalts are quartz normative, while basalts from other fields are typically olivine normative. In a seeming paradox, hand samples of Ricardo basalt appear to contain phenocrysts of olivine. Thin sections reveal, however, that only remnants of olivine remain; most grains having been replaced and pseudomorphed by iron oxides, siderite and iddingsite. Similar remnant olivines from the Big Pine field have been characterized as partially digested xenocrysts. Perhaps the altered olivines of the Ricardo basalts represent a reaction between an earlier alkaline magma that mixed with a pulse of later, more tholeiitic magma.

Trace elements were plotted on a Spider diagram and compared to other fields. The dramatic variations seen for major elements are less apparent. In general, all Mojave fields display a characteristic barium spike and incompatible element enrichment relative to the MORB standard. Ricardo basalts are slightly depleted in some incompatible elements, but the trends are less well defined than those for major elements. Trace element data suggests a common parentage and/or tectonic setting for all Mojave basalts. Minor differences can be attributed to mixing, assimilation or chemical variation

of source rocks.

Any model that relates Mojave basalts must explain the major element variations. Wang (2002) proposed that Cenozoic basalt composition varies from east to west across the Mojave as a function of depth of melting. To the east, magmas tapped deeper fertile mantle having higher alkali and incompatible trace element concentrations. To the west, shallower melting resulted in more siliceous, alkali-poor magmas derived from a depleted mantle. My data appears to support this hypothesis.

Introduction

Red Rock Canyon State Park is situated approximately 24 miles north of the town of Mojave, California. It contains one of the most interesting volcanic basalt fields, the Ricardo volcanics. Figure 1 shows the location of the Ricardo field as well as other basalt fields in the northern Mojave and southern Owens Valley.

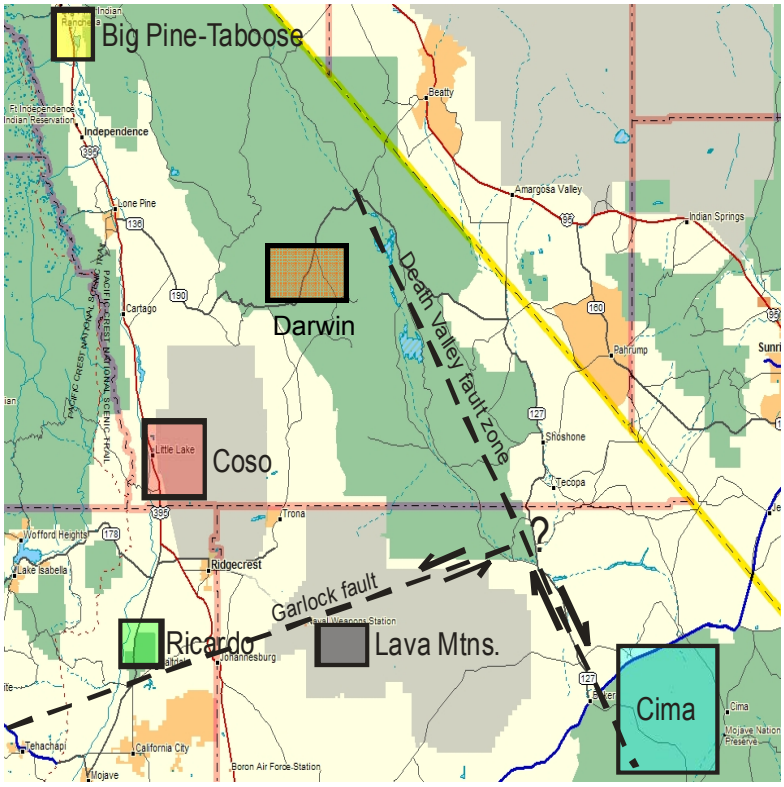

Figure 1. Index map showing the locations of selected Mojave basaltic volcanic fields.

Figure 2 outlines the approximate boundary of the study area, in essence, Red Rock Canyon State Park. The study area lies at the southwest end of the El Paso Mountains. It is easily accessible by California Highway 14 (CA 14) which cuts through the center of Red Rock Canyon State Park.

Many studies have been done on Mojave volcanic fields. Specifically, basaltic lavas have been exclusively studied in an effort to understand their petrogenesis. These studies have examined the isotopic and geochemical signatures in an effort to model the genesis and evolution of Mojave basalts. Furthermore, this data was thought to shed important light on the history and composition of the Earth's mantle beneath southern California.

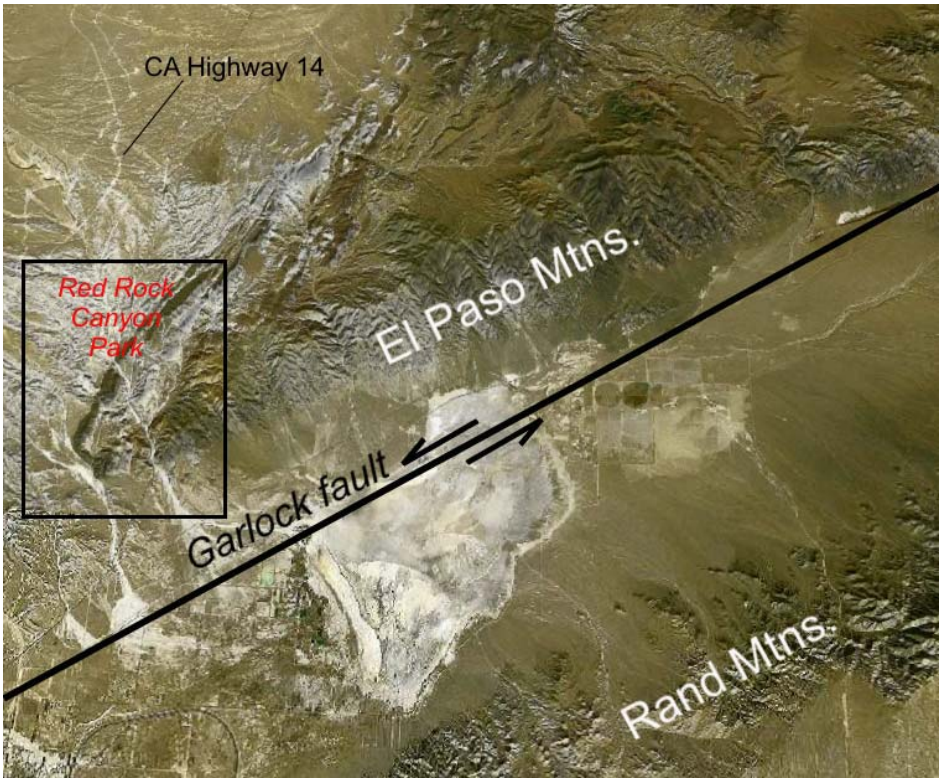

Figure 2. Satellite image showing the major geologic features of the Red Rock Canyon area (satellite image copyright Delorme, 2001)

Basalts can do this because they contain xenoliths that represent samples of original, unaltered mantle. This can give us an understanding of how the mantle formed and what comprises it. Another question that can be addressed by studying basalts is if the parental magma shows evidence of evolution with time. Trace elements can provide the best indications of magma evolutionary trends. Among the researchers who have studied basaltic lava fields in Southern California are Waits, (1995), Groves, (1996) and Darrow, (1972).

The Red Rock Canyon State Park is an ideal area to study basaltic lava flows and their relationship to the surrounding Mojave province. The area is relatively small and all of the unique rock features are reasonably accessible on foot or by vehicle. Another key feature is that the rock layers are not steep, so no heavy climbing is required. The geology is relatively straightforward in that there is not a lot of folding and faulting to distort the layers. You can see geology ranging from the Precambrian to the Holocene. There are adequate age constraints (K/Ar dates), however, there have been few

scientific papers published and no comprehensive geochemical or petrologic study of the basalt flows. Therefore, the work done for this research paper is somewhat new and innovative.

My initial goal in analyzing these samples is to determine the type of basalt present, requiring thin section examination and major element geochemistry. As a secondary goal, I would like to look at trace element geochemistry to determine if there is a unique chemical signature for Ricardo basalts. Furthermore, I would, perhaps, like to shed some light on the spatial relationship of the Ricardo basalts to other Mojave fields. As there is no visible vent in Red Rock Canyon area, have the Ricardo volcanics been moved into the area by offset along the El Paso or Garlock Fault, or was the magma chamber in situ? Therefore. I believe Red Rock Canyon is an ideal senior thesis project area to study geochemical and petrographic variation in basaltic lava flows.

Regional Geology

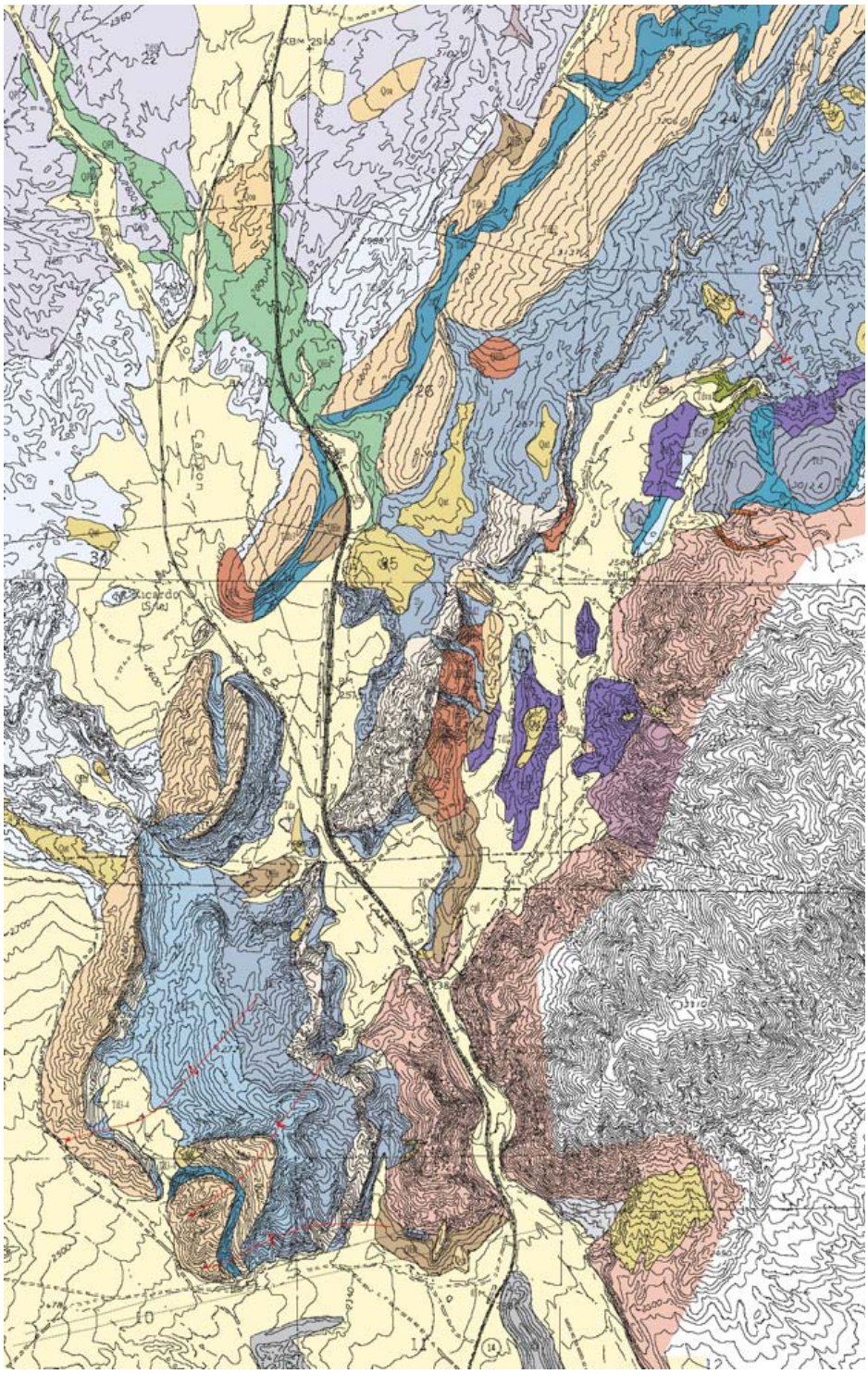

Figure 3. Detailed bedrock geologic map of the El Paso Mountains (Carr, M.D., et. Al., 1997)(Unit lithologies referenced by color in the text.).

People wandering through Red Rock Canyon State Park probably wonder how those magnificent red cliffs came into being. The answer is simple; it's geology and erosion. They represent a part of the half billion-year-old history of California. Since geologic time is measured in thousands of years, people can't directly observe these processes, only the results. In geology, the his-

tory of the area always starts with the oldest first and works its way to the present.

The oldest rocks exposed in this area are located in the central part of the nearby El Paso Mountains (Fig. 3). They are highly metamorphosed chlorite-quartz-albite-sericite Mesquite Schist. This Precambrian schist forms the basement upon which the weakly metamorphosed Late Paleozoic, marine Garlock Formation has been deposited. (Whistler, 1987). Deposition of the Garlock occurred approximately 225 million years ago.

The Garlock Formation consists of shales, cherts, limestones, conglomerates, quartzites, and subaqueous volcanic flows. These are not seen in the Red Rock Canyon area, but in the northeastern portion of the El Paso Mountains. The Paleozoic seabed began slowly rising due to crustal movements initiated around 200 million years ago, culminating with the instrusion of granitic batholiths. The “complex of plutonic rocks range in composition from hornblende-quartz diorite to granite. One of these intrusive units, a highly fractured and jointed granophyre plug, surrounds the gorge at the entrance to Red Rock Canyon.” (Whistler, 1987). These are the oldest rocks that are seen in Red Rock area itself. The age of the rocks is believed to be around 100 ma.

“No rocks in the Red Rock Canyon area record the events between 100 million and 58 million years ago. However, the Garlock Fault, which would have a dominant influence on the subsequent geologic history of the area, developed nearby during this time.” (Whistler, 1987). The Garlock Fault is one the largest faults in California. Geologists believe you can trace the fault for approximately 250 kilometers across the northern part of the Mojave Desert. “The Garlock Fault is a major transform fault which

separates the relatively stable Mojave Block to the south from the major crustal extensional area of the Basin and Range Province to the north." (Whistler, 1987). It is thought to have left-lateral displacement around 48 to 64 kilometers. Evidence for movement can be seen in alluvial fans at the front of the El Paso Mountains that have been displaced approximately 18 kilometers during the past 1.5 million years.

A splay of the Garlock Fault, the El Paso Fault, is responsible for the uplift of the rocks in Red Rock Canyon. Since part of the geologic story is missing, total uplift cannot be accurately calculated but is believed to be around 3000 meters.

Near the end of the Paleocene Epoch (around 58 million years ago), streams from the north started to erode the area. The streams carried boulders and gravels from the north/northeast into the newly formed valleys of the uplifted area of the El Paso Mountains. The stratigraphic history records this as the Paleozoic and Mesozoic rocks are deeply eroded and are unconformably overlain by continental clastics of the Goler Formation of Paleocene age (Whistler, 1983) These stream and lakebed deposits are approximately 2200 meters in thickness. The Goler Formation does not outcrop in Red Rock Canyon itself, but is found in the nearby Scenic Canyon, which is on the eastern side of the study area.

The next forty million years of geologic history are poorly understood since there's no geologic record in Red Rock Canyon. However, around 18 million years ago, the western Mojave became a center of volcanism. The volcanic flows and ashes that resulted are called the Tropico Group. Part of the Tropico Group consists of airborne ash falls and tuff breccias. Much of the ash was washed into surrounding streams and lakes to form volcanic mud. The Tropico Group is generally thought to be

Middle Miocene in age.

The Middle Miocene basal sequence includes "coarse pyroclastics and andesite flows that are most prevalent in Last Chance Canyon in the west-central El Paso Mountains. They also form most of the rocks of Black Mountain in the northwestern El Paso Mountains." (Whistler, 1987). The age of these are thought to be between 15 to 19 million years old. "The last pulse of this Middle Miocene volcanic episode was the outpouring of andesite breccia lava flows. The andesite dikes, can be seen in Last Chance Canyon. These andesite breccia flows form the top of Black Mountain, the high point in the El Paso Mountains, and can be traced continuously to within one mile of Red Rock Canyon." (Whistler, 1987).

Figure 4. Ridge-capping Ricardo basalts dipping to the northwest with underlying lacustrine sediments; view to the northwest.

The next event to occur in the Late Miocene is the one in which various sediments were deposited in channels cutting the Tropico Group. This was the beginning of deposition of the Ricardo Formation (Fig. 4). The Late Miocene deposits consist of lacustrine and fluviatile sediments. "These form the scenic, multicolored badlands in

Red Rock Canyon. The lower 800 meters of this succession contain numerous volcanic ash falls, two thick lapilli tuff breccias and two basalt flow sequences. " (Whistler, 1987). The source of all the cliff-forming sediments seems to lie to the east.

Nearby volcanoes influenced the landscape later in the Miocene Epoch by blanketing the surrounding areas and essentially "capping" the lacustrine sediments. In all there were 25 to 30 different lava and ash falls. "Some of these form the ridges which dominate the area today, including the red cliffs near the entrance to Red Rock Canyon capped by pink and yellow tuff breccia. This cliff-forming bed continues over 10 kilometers to the north." (Whistler, 1987). The ashes in the area are seen as white bands in Last Chance Canyon. Since the ash is easily seen, it's often used as a stratigraphic marker. The dates from these ashes are between 8-10 million years.

Subsequent to deposition of the Ricardo Formation, the El Paso Mountains were uplifted approximately 2000 meters along the El Paso Fault and the Ricardo Formation was tilted 25 degrees to the northwest. Because of this, there is no Ricardo Formation at the top of the El Paso Mountains.

The area was then inundated with stream and alluvial fan deposits from the Sierra Nevada Mountains; the basalt and tuff breccia are the only rocks that were not buried by the sediments. The alluvial fans have been dated at around 25,000 years. You can observe the remnants of the alluvial fans near the Red Rock Campground. The latest erosion started between 1,000 to 2,000 years ago. This erosion is responsible for cutting the scenery seen today. The El Paso Fault remains active uplifting the area from time to time. Therefore, Red Rock Canyon continues to be actively shaped today.

My research is focused on the basalts of the Ricardo Formation. Table 1 shows the postulated ages for Ricardo basalts as well as ages for nearby Mojave basaltic volcanic fields.

Table 1. Ages of Mojave Basalts

- Ricardo (Red Rock) 8.2—10.1 Ma
- Darwin 6—8 Ma
- Coso Recent—2.5 Ma
- Big Pine 0.25—2 Ma
- Cima Recent—6 Ma

As the table shows, the Ricardo volcanics are Miocene in age. The Darwin Field is very latest Miocene; the Cima Volcanics range from Miocene to recent, while Coso and Big Pine are Plio/Pleistocene to recent in age.

There are many important tectonic features in the vicinity of Red Rock Canyon State Park. The first is the Death Valley Fault Zone, which lies to the northeast. This fault zone is characterized by right slip although the timing and amount of movement is uncertain. Immediately to the south of the Ricardo volcanic field is the Garlock Fault. This fault is approximately 250 kilometers long, striking roughly east-west from the San Andreas Fault to the Death Valley Fault Zone. It separates the Basin and Range geomorphic province to the north from the Mojave Desert geomorphic province to the south. Tensional forces acting on the Basin and Range province during the Cenozoic Era have caused the area north of the Garlock Fault to move westward relative to the Mojave Desert block, thus, the sense of the slip on the Garlock Fault is left lateral. The

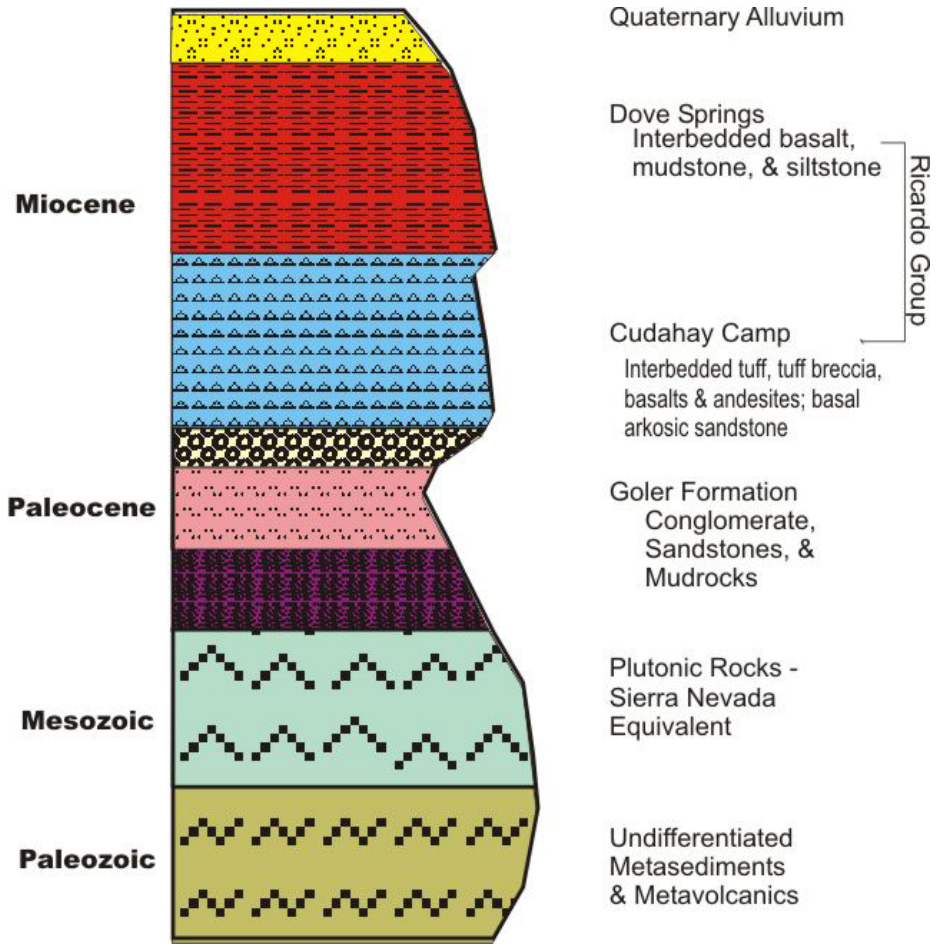

Figure 5. Stratigraphic column for the southern El Paso Mountains.

maximum offset along the fault ranges from 50 to 70 kilometers and with all movement occurring in the last 8 to 9 million years.

Now, let's take a closer look at the rocks that make up the study area (Fig 5). The older basement rocks lie in the east-southeast portion of the study area. These are Mesozoic plutonic rocks (granites) of the Sierra Nevada batholith. The northwest-striking Miocene Ricardo Group, consisting of twenty-five Miocene volcanic flows/falls with interbedded fluvial/lacustrine sediments (colored blue, peach, and dark blue on the geologic map), lies in disconformable contact with the basement rocks. Basalts generally form the ridge caps, with poorly cemented ash flows and lacustrine units un-

derlying the valleys.

The volcanic layers within the Ricardo consist of twenty-three basaltic to andesitic flows. There are also pyroclastic flow and fall deposits, which are generally rhyolitic in composition. The latter have been used to age date the Ricardo volcanics at 8.2 to 10.1 Ma. Near the top of the Ricardo group is a tuff that was used to make the famous Dutch Cleanser. The other units inherent to the Ricardo group are fluvial and lacustrine rocks whose compositions range from conglomerate at the base to mudstone or siltstone up section.

The Ricardo Formation has been recently elevated into group status and two formations defined: Cudahay Camp (Fig. 6) and Dove Springs (Fig. 7). The Cudahay Camp unconformably overlies the Goler Formation. It consists predominantly of volcanic tuffs and coarser grained clastics. Directly above is the Dove Springs group consisting of basalt flows, tuffs, and finer clastic sediments.

Figure 6. Upper Dove Springs Member of the Ricardo Formation, exposed along California Highway 14, near the Ricardo Campground.

Figure 7. Felsic tuffs and basalts of the Cudahay Camp Member, Ricardo Formation, Last Chance Canyon.

Petrography

Hand samples were collected for laboratory study and thin sections prepared for microscopic examination. Thin sections were made by Quality Thin Sections of Tucson, Arizona.

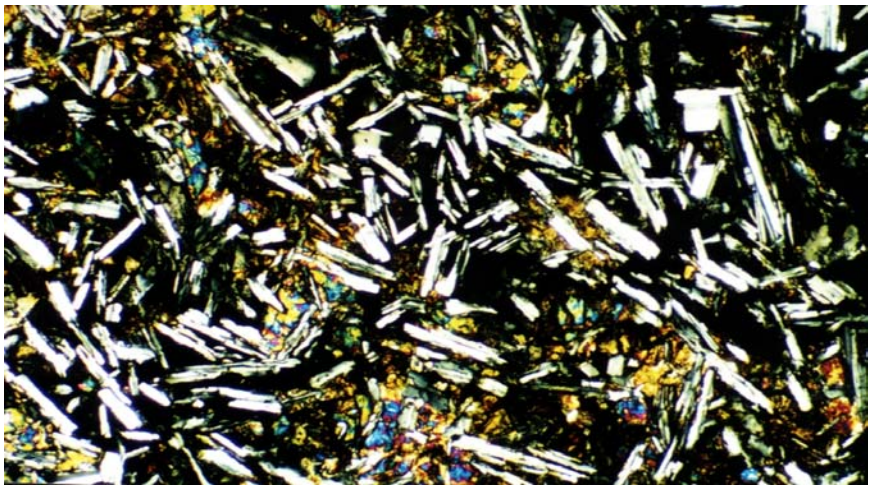

Figure 8. Thin section showing the typical plagioclase grains found in the Ricardo basalts. Polarized light, 10X magnification.

Thin section examination (Fig. 8) revealed that Ricardo basalts are generally comprised of 1-1.5 mm, euhedral, plagioclase crystals set in a matrix of skeletal pyroxene and glass. Occasional, large (5-10 mm) phenocrysts of augite and highly altered (1-3 mm) phenocrysts of olivine are also present. In many cases only the cores of olivine grains remain unaltered, the rims consisting of iddingsite and hydrated iron oxides. This presents a paradox, since geochemical analy-

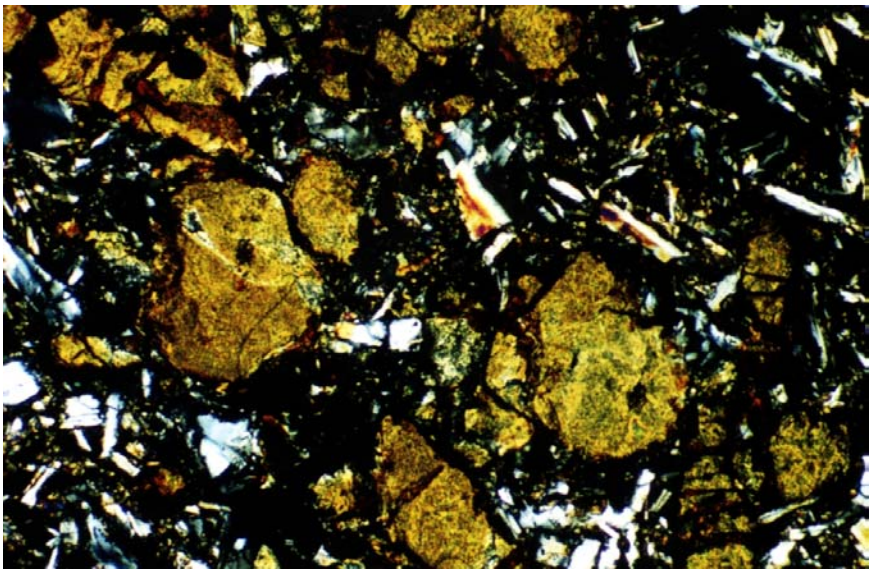

Figure 9. Photograph showing the altered olivine phenocrysts that appear in some of the Ricardo thin sections. Polarized light, 10X magnification.

ses suggest Ricardo basalts should NOT contain modal olivine. Locally, Casiderite completely replaces and pseudomorphs olivine as is shown in Figure 10. The alteration of olivine suggests that it may represent a xenocrystic phase. Subsequent reaction with the magma altered the olivine to iddingsite/siderite. Perhaps the olivine xenocrysts were engulfed by a more siliceous pulse of magma which was then extruded before digestion of the olivine grains was complete. Darwin (1972) studied the basalts of the Big Pine field and found similar olivine xenocrysts. He suggested these were inherited from an earlier magma. Winter (2001) states that resorbed olivine with orthopyroxene reaction rims can occur in tholeiitic basalts (see Geochemistry discussion). Another possibility that must be considered is some form of subsequent alteration of the Ricardo basalts, perhaps due to hydrothermal or meteoric fluids. The latter is unlikely since many of the samples showed little or no visible alteration; even the characteristic iron oxidation was not present in the fresher outcrops adjacent to California Highway 14. The former possibility, however, cannot be discounted. Cer-

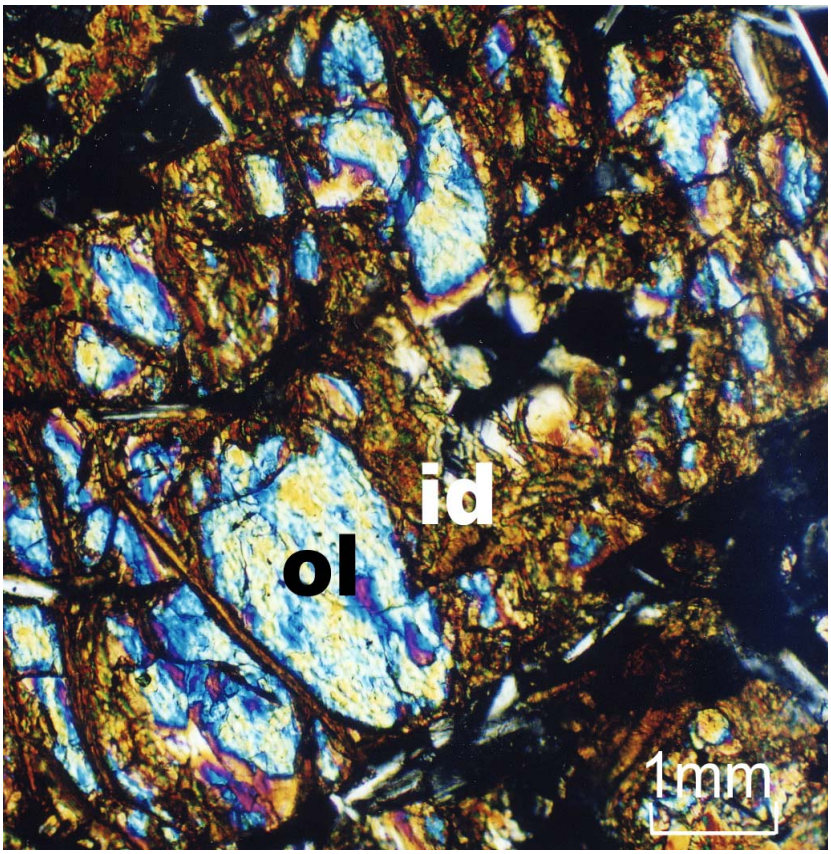

Figure 10. Photograph showing olivine (ol) altering to iddingsite (id). Polarized light.

tainly, hydrothermal fluids played a role in borate mineralization in many localities throughout the Mojave. These same fluids could have altered nearby basalt fields.

Sample Preparation for Geochemical Analysis

The first step in sample preparation was to cut the hand sample down to a size that would fit into a Chipmunk jaw crusher (<8cm). The actual cutting was performed by using a diamond saw. The sample was then placed into the steel jaw crusher. After the sample has been crushed, it is poured into a sample splitter. The splitter reduces the sample volume to that necessary for ball milling. The sample is then put into a holder for the ball mill. After the sample has been secured in the holder, the ball mill is run for 30 minutes. After 30 minutes, the sample is sieved through a –60 micron sieve. The oversized sample is reground for approximately 15 minutes. Ideally 50% of the sample should pass through the fine mesh sieve.

Once the sample has been sieved, it is then made into a "pellet". Six grams of sample are weighed onto an analytical balance and 1.2 grams of cellulose binder is added. The sample and binder are then mixed in the ball mill, without a steel ball, for approximately 1-3 minutes. The next step involves pelletizing the powdered sample using a die and press. Initially, an aluminum cup is placed in the die and the sample poured in. The sample is compacted by hand and then placed in a hydraulic press where the pressure is pumped up to 15 tons. It is allowed to stay in the press for one minute and the pressure released. The result is a flat, disc-shaped "pellet". All samples were prepared in this manner.

The pellets are then placed into the x-ray spectrometer. The spectrometer analyzed the samples using whole rock and trace element computer programs. Every sample was analyzed utilizing the whole rock analysis based upon the USGS Standards. This measured the major elements present in each sample (Si, Al, Ca, Mg, Fe,

Mn, Na, K, P, Ti). After this program run was completed, the sample data were examined for each sample and those that had SiO_2 percentages below 58% (categorized as basalt) was placed back into the x-ray spectrometer and run through trace element analyses. Trace elements were analyzed utilizing a program created by Dr. David Jessey at Cal Poly University, *basalt_trace*. The elements that were analyzed were Ba, Ce, Cr, La, Nd, Rb, Sr, Sc, Y, Zr, and Sm. Lastly, Dr. Siegel of the Cal Poly Physics Department analyzed some basalt samples to measure their Thorium and Uranium contents.

After data had been collected for all samples, a computer software package, Ig-Pet 2001, was used to make the petrographic diagrams discussed in the subsequent section. This program allows one to make a wide variety of diagrams, however, only those diagrams that provided the best representation of the Ricardo basalts were selected for inclusion in this thesis. What follows is a discussion of both major element and trace element geochemistry.

Geochemistry

Major element data for the Ricardo volcanics can be found in Appendix A; trace element data for the basalts in Appendix B.

Figure 11 summarizes the compositional variation within the Ricardo volcanics. Notice that nearly all Ricardo volcanics lie within the typical basalt-andesite-dacite-rhyolite lineage. LeBas proposed that alkalis were the key elements to enable classification and discrimination of a volcanic rock. Utilizing the LeBas diagram, the Ricardo volcanics are true basalts, not trachybasalts like other Mojave basalt fields. Ricardo volcanics have a higher percentage of silica and are lower in the alkalis when compared to Coso, Cima, and Big Pine. The diagram also shows that some of the basalts of the Ricardo field are basaltic andesites. Table 2 is a CIPW normative analysis calculated for all Ricardo rocks containing less than 58% SiO_2 (basalt and basaltic andesite). The CIPW analysis indicates that the Ricardo basalts are quartz normative; containing no normative olivine making them tholeiites. It is im-

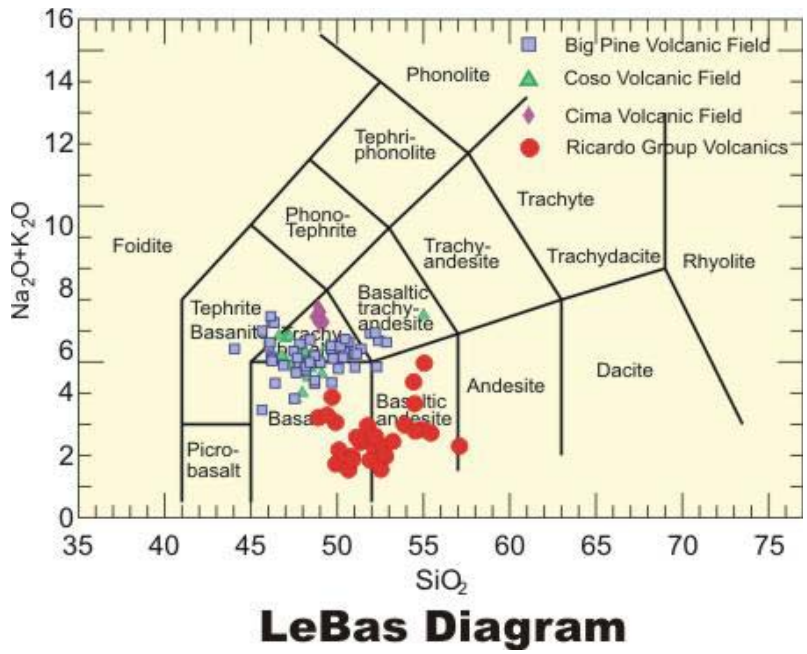

Figure 11. LeBas Diagram showing basalts from Big Pine, Coso, Cima, and Ricardo fields.

Table 2. CIPW Normative Analysis - Ricardo basalt

Mineral	*Normative wt %*
Q	**11.8**
or	7.6
ab	19.8
an	26.9
ne	0.0
di	13.8
hy	14.8
ol	**0.0**
mt	3.0
il	1.8
ap	0.5

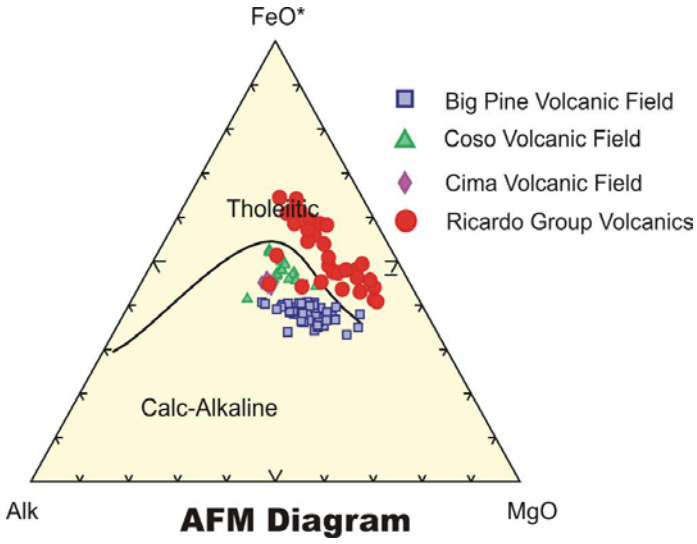

Figure 12. An AMF diagram for all of Mojave basalts.

portant to note that all other Mojave basalt fields for which data are available (Darrow, 1972, Groves, 1996 and Waits, 1995) have been characterized as olivine normative.

Figure 12 is an AMF diagram for Mojave basalts. It contrasts basalts from the Coso, Cima, and Big Pine fields to those of the Ricardo group. The samples from the other volcanic fields show distinct differences when compared to the Ricardo volcanics. Ricardo seems to be the only truly tholeiitic field. The others plot in the calc-alkaline field. In this instance, calc-alkaline is a stand-in for all alkaline rocks, so that the others are really alkaline (olivine normative), not necessarily calc-alkaline.

Figure 13 is a basalt tetrahedron (Yoder and Tilly Diagram) for several Mojave

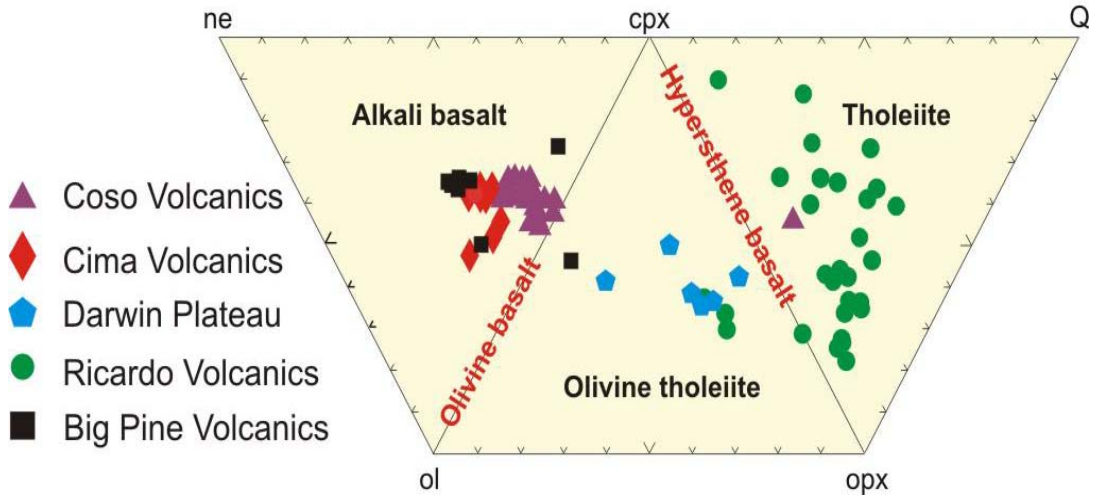

Figure 13. A basalt tetrahedron for Mojave basalts. Data from Groves (1996), Waits (1995), Darrow (1972), Cal Poly Geochemistry class (2001) and this thesis.

basalt fields. It plots normative quartz (Q), orthopyroxene (opx), clinopyroxene (cpx), olivine (ol), and nepheline (ne). In this diagram, the differences between the basalt fields are more pronounced than in either the AFM or LeBas diagrams. The Ricardo volcanics plot in the tholeiite field. Coso, Cima, and Big Pine mostly plot on the alkali basalt side. Darwin Plateau basalts seem to plot in the middle, which is the olivine tholeiite region. Combining the LeBas and Yoder & Tilly diagrams suggests an evolutionary trend of decreasing SiO_2 and increasing alkalis. These differences could be related to geologic setting or might even be age related (see Table 1). The Ricardo volcanics are Miocene in age, which is the oldest of the five volcanic fields. The Darwin Plateau is latest Miocene, and samples from the other three volcanic fields are Plio-Pleistocene in age. This diagram suggests that Mojave basalts may have evolved from older tholeiites to younger alkaline basalts. I shall revisit this question in the Discussion section of my thesis.

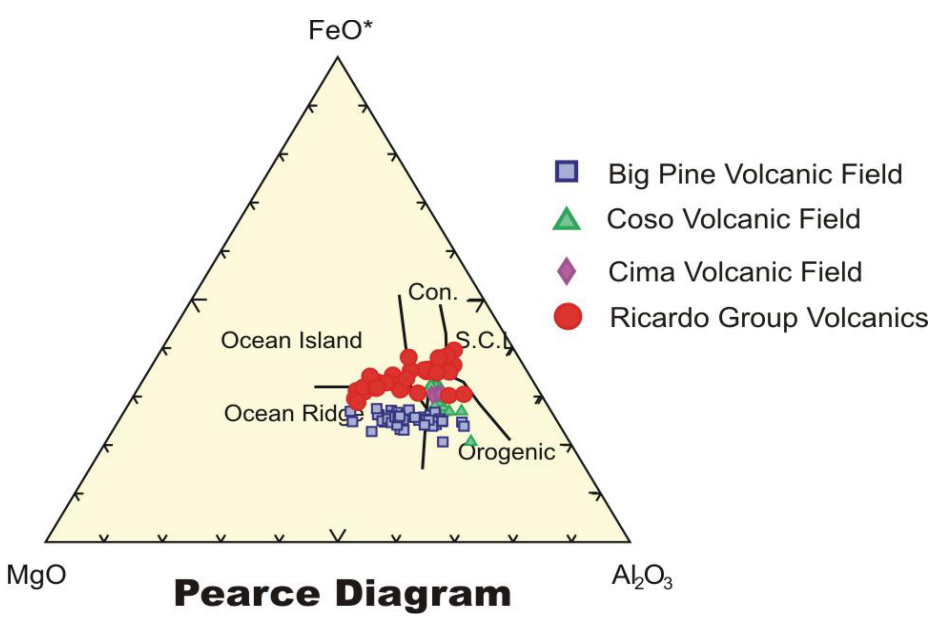

Figure 14. Pearce diagram showing a plot for Mojave basalts.

Pearce & Mullen diagrams have found increasing use over the past few decades. Both are thought to be sensitive indicators of tectonic environment are often utilized in petrogen-

tic interpretation.

The Pearce diagram (Fig.14) plots FeO* (FeO + Fe_2O_3) vs. MgO, and Al_2O_3. For this particular diagram, Big Pine, Cima, Coso, and Ricardo volcanics have been plotted. The Pearce diagram isn't particularly helpful for the Ricardo volcanics. The Ricardo basalts plot across a wide range and cannot be well characterized. The other volcanic fields are more consistent and appear to be ocean ridge/orogenic (OIA). The best that can be said is that the Ricardo volcanics appear to be dramatically different than the other Mojave fields.

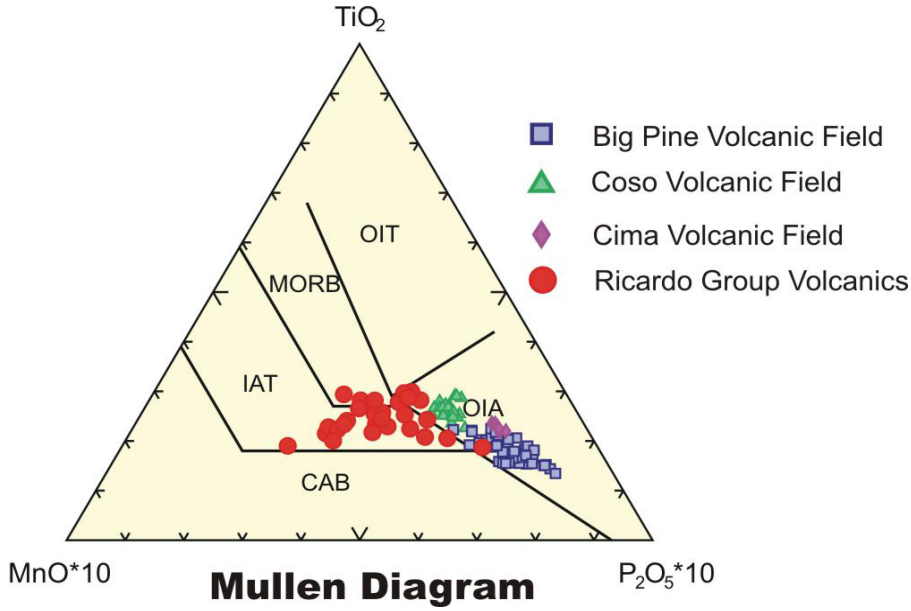

Figure 15. Mullen diagram for the Mojave basalts.

The Mullen diagram (Fig.15) appears to be more useful. In this diagram, TiO_2, MnO*10, and P_2O_5*10 are plotted. In the case of the Mullen diagram, the Ricardo volcanics are largely restricted to the MORB (Mid-Ocean Ridge Basalt)/IAT (Island Arc Tholeiite) fields. The Cima, Coso, and Big Pine volcanic fields lie mostly in the OIA (Ocean Island Alkaline) field. This apparent alkaline trend for both Cima and Coso has been noted in previous publications on Mojave volcanic fields.

The final geochemical diagram is a Spider diagram (Fig.16). Essentially, it plots trace and minor elements for an idealized MORB against trace and minor element contents from Mojave fields. This diagram was generated using the *basalt_trace* program created for the XRF by Dr. David Jessey. The MORB standard values are from Sun and McDonough (1972). The thorium values are from energy dispersive spectroscopy and were provided by Dr. Peter Siegel, Cal-Poly Physics Department.

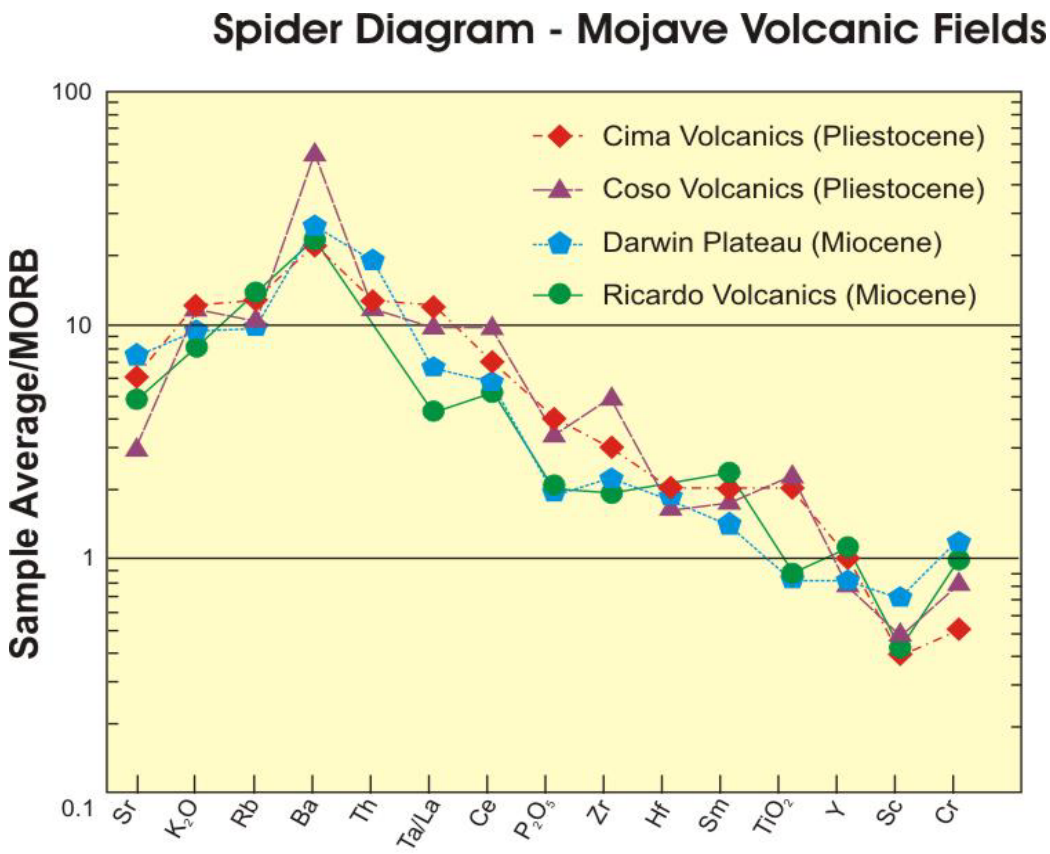

Figure 16. Spider diagram showing trace element content of the Mojave basalts. Standards are those of Sun and McDonough (1972).

Trace and minor elements are often more sensitive indicators of petrogenesis than are major elements. In other words, those rocks, which share a common source should plot similarly. Rb-Ba are the represent most incompatible elements in all ba-

salts, with incompatibility decreasing in either direction away from those two elements. Note that all of the Mojave volcanic fields look quite similar to one other. Darwin and Ricardo may be slightly depleted relative to the other fields, but this is just an educated guess. It's hard to make a concrete argument from this diagram. Note, also, the characteristic Mojave barium spike, meaning all Mojave basalt fields are anomalously high in barium relative to the MORB standard. The high barium content of Mojave volcanics has long been known. No reason has ever been given for the barium anomaly.

To briefly summarize, the Spider diagram suggests that the Ricardo basalt field shares a common genetic/tectonic ancestry with other Mojave volcanic fields. Thus, the major element differences noted previously, can't be due to a radically different plate tectonic setting. Ricardo basalts must have a similar source and be related genetically to other Mojave volcanic fields.

Discussion

To better understand the petrogenesis of basalts, let's examine a diagram, which shows the possible different source areas for basaltic magma (Fig.17).

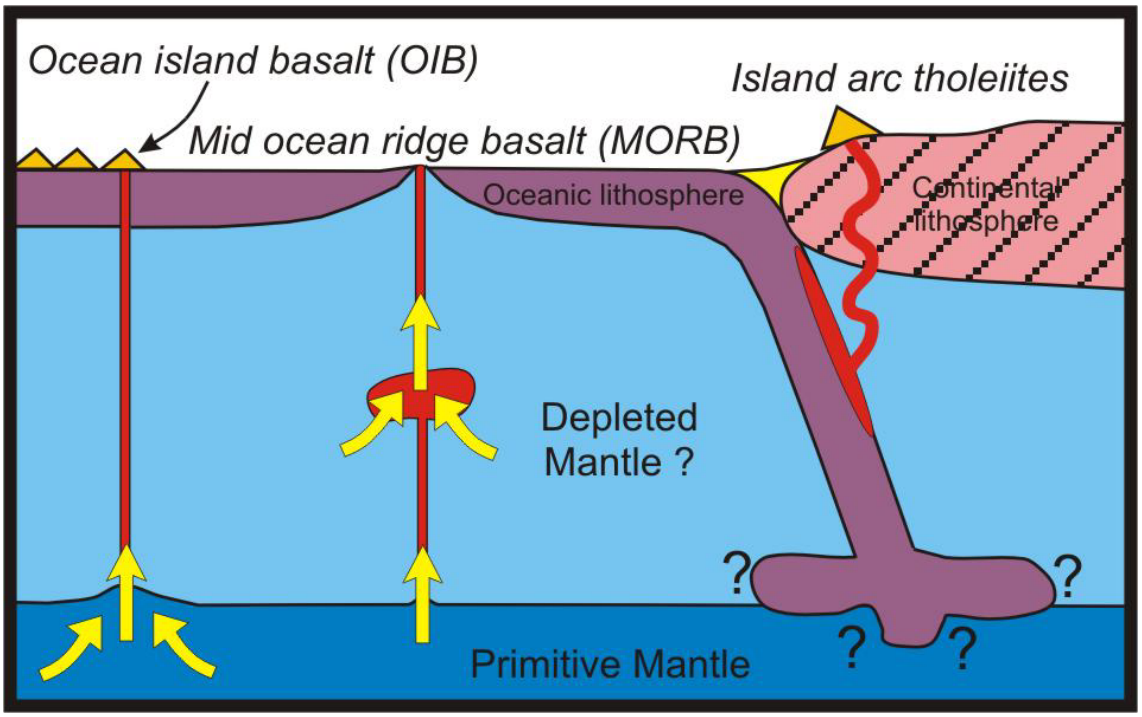

Figure 17. Cartoon sketch showing the four possible sources of basaltic magma.

There are four possible sources:

- Ocean Island Basalts (OIB) - thought to be generated from deep-seated mantle plumes that melt fertile (primitive) mantle and do not interact with the shallow depleted mantle.
- MORBs - of which there are two subtypes:

  - N-MORB—a Normal Mid-Ocean Ridge Basalt (tholeiite), thought to have originated in an upper depleted layer of the mantle that has gone through repeated recycling during plate tectonics.

  - E-MORB—(enriched MORB) - more controversial, but probably the result of

magma mixing, and containing both depleted and primitive mantle.

- Island Arc Tholeiites (OIT) - form at a convergent margin as a consequence of plate subduction. They are highly variable in composition, but often have higher silica content and enrichment in crustal contaminants.

The following diagrams (Fig.18) compare Ricardo volcanics to those for model basalts that are generated from the four different possible magma sources.

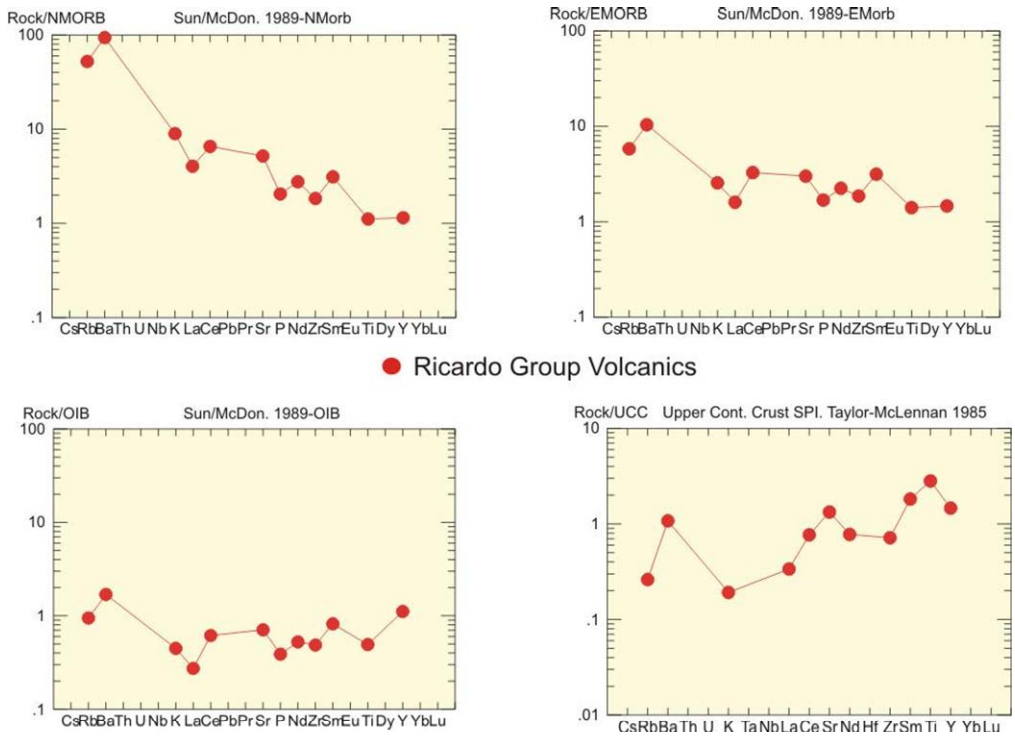

Figure 18. A comparison diagram of Ricardo volcanics to model basalts from the four possible magma sources.

For a volcanic field to “best fit” a standard, it should have values close to or slightly greater than “1” for all trace elements. It appears that the Ricardo volcanics most closely resemble an E-MORB. The N-MORB can be dismissed because the Ricardo volcanics are too enriched relative to the standard.

The OIB appears to also be a good fit. However, the Ricardo volcanics are depleted relative to some elements in the OIB. This suggests that it can't be related. Why? Because if we melt a rock, the most incompatible elements leave the quickest. Therefore, if the rock lies below the standard, it suggests our magma source had to be different. In other words, if the OIB represents the "melted" source, we should see enrichment in the most incompatible elements in the Ricardo volcanics. Clearly, we do not.

UCC is used as a stand-in for ocean island tholeiite (there is no OIT standard). The positive slope for the graph argues against a relationship between Ricardo volcanics and UCC. The Ricardo volcanics are enriched in the more compatible elements than the UCC. If Ricardo volcanics are a consequence of plate subduction, they should be depleted in the more compatible elements relative to the standard. Instead, they are enriched. The source tends to lose incompatibles and retain compatibles. Thus, a UCC source is highly unlikely.

What does this all mean? It would seem the Ricardo volcanics are MORB tholeiites, perhaps the slightly enriched E-MORB variety. All of the other Mojave basalts are distinctly more alkaline (Ocean Island Basalt-like).

How can we get compositionally different basalts? There are three possibilities. The first could be a true compositional difference in the mantle source. This would have to be minor if we are looking at the same tectonic setting, but could vary dramatically if we change the tectonic setting. The second possibility could be differences in the percentage of partial melting that has occurred. Third, the compositional difference could be due to depth of melting. We can ignore the first

possibility for two reasons. First, Ricardo volcanics overlap the ages of other fields and hence, it is difficult to imagine a vastly different tectonic setting for vvolcanic fields in such close geographic proximity. Also the Spider diagram shows a strong genetic/ tectonic relationship between fields.

Therefore, we need to look at how it is possible to generate compositionally different basalts in the same tectonic setting. One possibility is by varying the degree of partial melting.

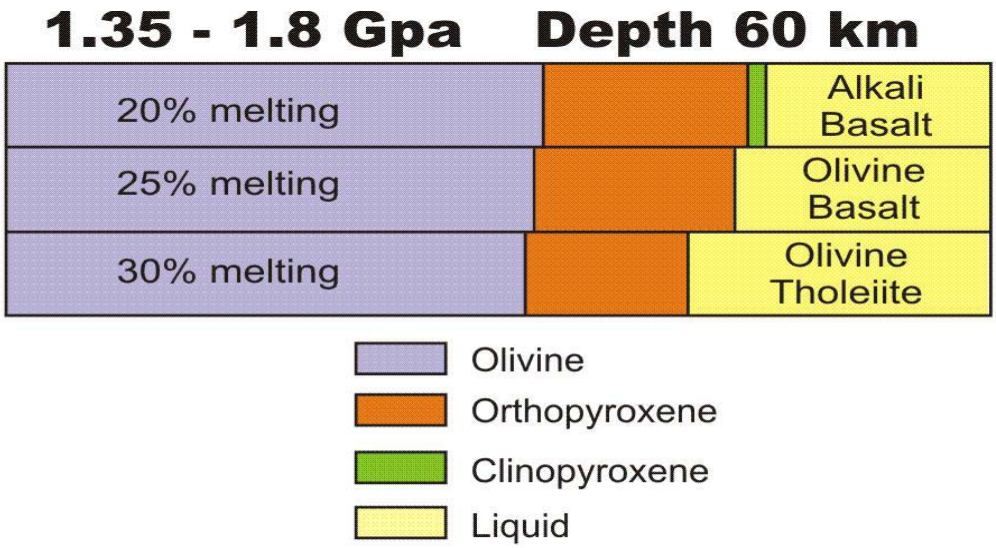

Figure 19. Relationship between partial melting and basalt composition. After Ringwood (1976).

Figure 19 compares basalt composition and the percentage of partial melt. Ringwood (1976) showed that if we maintain depth as a constant, we can vary the composition of the melt that we extract from the primitive mantle by varying the amount of partial melt. At 20% partial melt, we get an alkali basalt like Cima, Coso, or Big Pine. At 30% partial melt, we get an olivine tholeiite, like the Darwin Plateau. How do we vary the percentage of partial melt? One mechanism would be to vary the temperature. Higher temperature will yield a greater percentage of melt. The second

way to vary the partial melt percentage is to allow a longer period of melting.

Another mechanism to change the composition of the extracted basaltic magma is to vary the pressure. Figure 20 shows the position of the eutectic (the composition of the first partial melt) as a consequence of changing pressure. Notice that at 1 atmosphere (atm), the eutectic lies within the albite, enstatite, and silica field yielding a tholeiitic magma. At 1 giga-Pascal (Gpa), we are in the nepheline, forsterite, albite field yielding an alkaline magma. Therefore, a lower pressure environment favors tholeiitic magma, while a higher pressure environment favors alkaline magma. Obviously, this would be a function of depth of melting since pressure varies as a function of depth. A shallow partial melt would be more tholeiitic, and a deeper melt would yield a more alkaline magma.

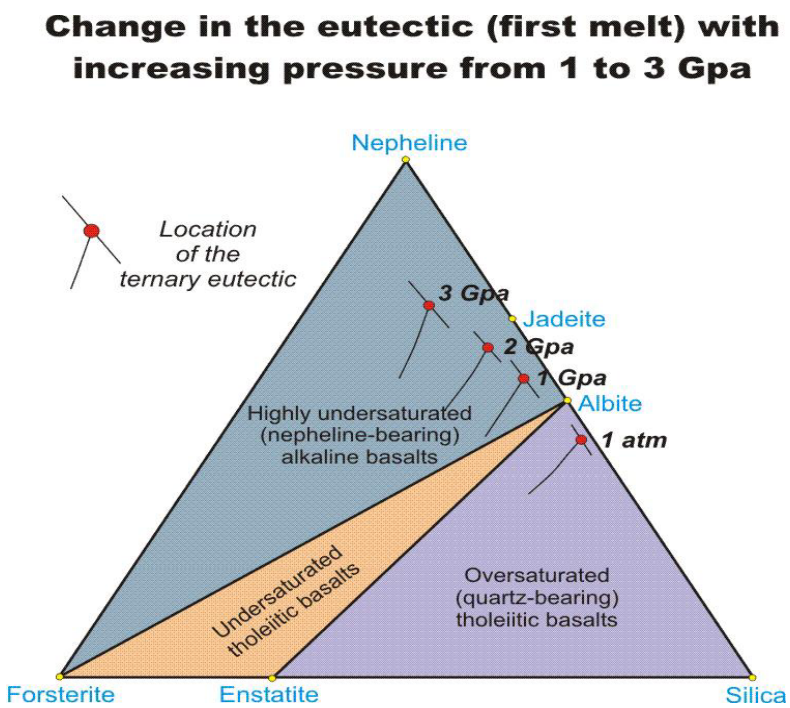

Figure 20. Diagram illustrating the change in eutectic composition (first melt) with increasing pressure.

In a recent paper by Wang and others (2002) it is suggested that melting depth for Cenozoic magmas varies dramatically from east to west across the Mojave. Red arrows (Fig. 21) represent his calculated depths of melting for various basalt fields. Wang used an Iron8 index to determine melting depth from the Colorado Plateau westward across the Mojave. Coso and Big Pine represent the westernmost fields in

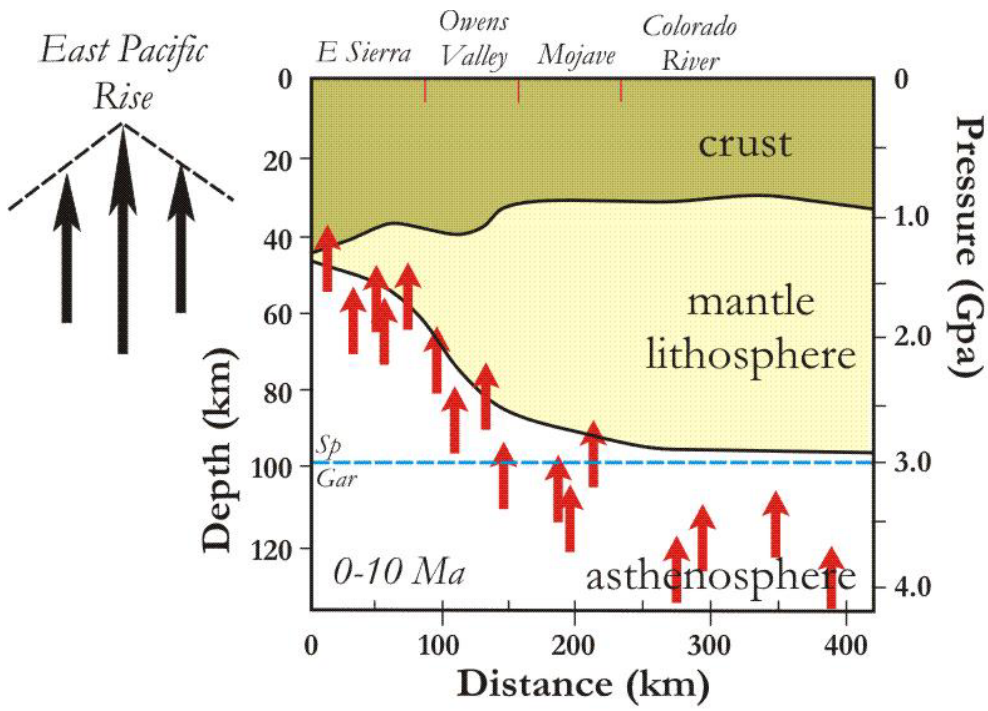

Figure 21. The melting profile for basaltic magmas across the western Basin and Range. From Wang (2002).

the study. (The Ricardo field lies another 30-40 km further to the west).

This diagram demonstrates that melting depth does vary significantly across the Mojave. Since the Ricardo field lies to the west of Wang's study area, it should represent the shallowest mantle melt. It also follows that it would be the most tholeiitic (remember shallow depth favors tholeittic magma). A cautionary note is that Wang's data was highly generalized and his projection onto the west-east cross section about the latitude of the Garlock fault is a little suspect. Some fields are well north or south of the cross section line!

Figure 22 is a suggested model for the genesis of the Mojave basalts. The cartoon sketch indicates that during the Miocene, the East Pacific Rise (EPR) was beginning to be subducted beneath continental North America. The Rise (spreading

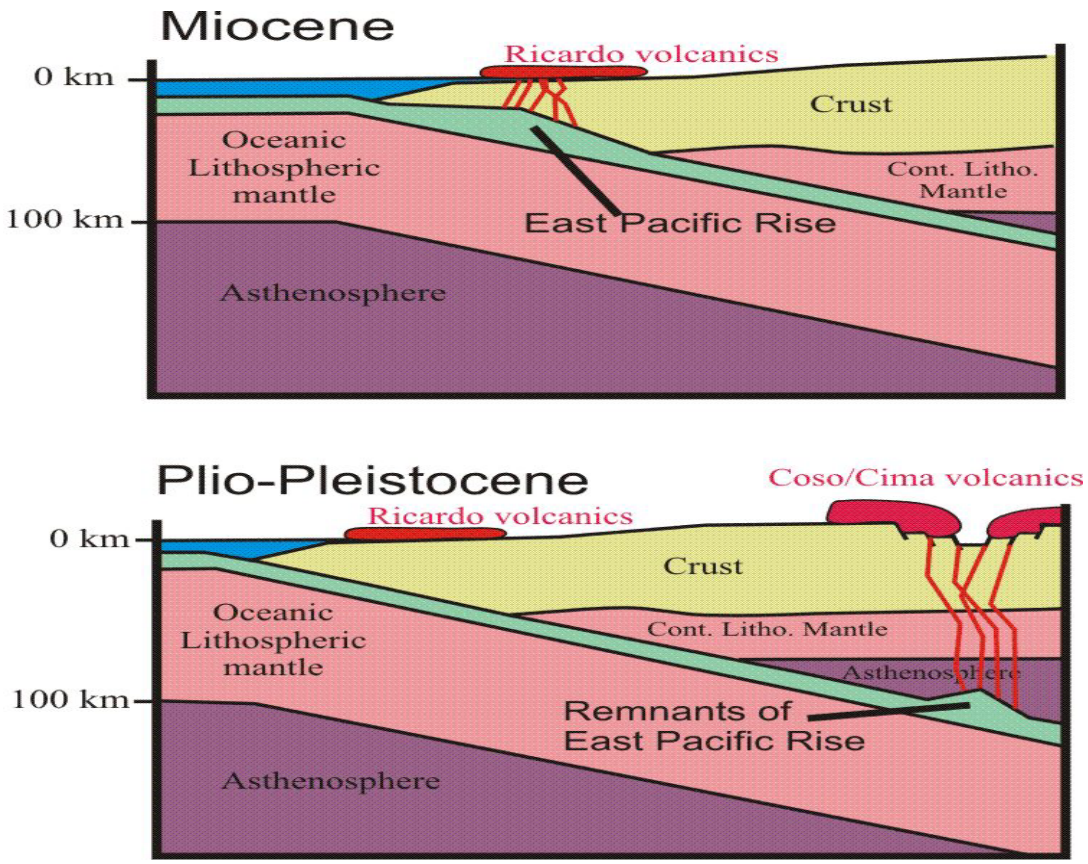

Figure 22. Cartoon sketch showing a suggested model for the genesis of Mojave basalts.

center) was still quite hot and at shallow depth. Hence, Miocene basalts were generated at shallow depth and nearer to the trench from the still-hot East Pacific Rise. The result is the MORB-like Ricardo volcanics. By the Plio-Pleistocene, the EPR had managed to work its way deeper and the heat source may have been waning. Greater depth and lower percentage of partial melt favored more alkaline magma similar to that of Coso, Cima, and Big Pine. Note, also, as we get deeper, we encounter the asthenospheric mantle wedge. This might cause the depleted Miocene MORB magma to mix with primitive mantle generating the more alkaline Coso and Cima fields. The bottom diagram also shows rather prominent extension. This is necessatated by the fact that isotopic studies have shown that no Mojave basalts contain significant crustal

contiminants. Therefore, Plio-Pleistocene basalts must have traversed the crust rapidly to avoid contamination; limiting emplacement to periods of extension.

In conclusion, the Spider diagram shows that all Cenozoic Mojave basalts have a common parentage. When the Ricardo volcanics are compared to model basalts they tend to be a slightly enriched mid-ocean ridge basalt (E or N MORB). Ricardo basalts have, in general, lower alkali content and greater silica content than other Mojave basalt fields (Coso, Cima, Big Pine, and Darwin). The Ricardo volcanics seem to be a product of greater residual heat from the East Pacific Rise during the Miocene which resulted in a higher percentage of partial melt. In addition, the shallower depth of melting to the west (nearer the trench) favored a more tholeiitic magma. Finally, the compositional difference (greater alkalinity) from other Mojave fields may also be a function of the incursion of mantle asthenosphere to the east, due to greater melting depth.

Suggestions for Further Research

- Big Pine has been shown to be contaminated by crustal material (isotope studies). Would detailed trace element studies identify signature contaminant elements that could be extrapolated to other fields? (saving expensive isotopic analyses)
- How do the basalts of the Long Valley Caldera and Mono Basin compare to those of the Mojave?
- Darwin Plateau trends are based upon only eight samples, would more extensive sampling reveal a broader spectrum of data linking the older and younger basalts?
- Cima volcanic field spans a time range from Miocene to Recent, yet only Pleistocene basalts have been extensively sampled. Would a comprehensive sampling project reveal a distinct trend of early tholeiitic rocks and younger, more alkaline rocks?

REFERENCES

- Coleman, Drew, and Walker, J.D., 1990. Geochemistry of Mio-Pliocene rocks around Panamint Valley, California, *in* Basin and Range extensional tectonics near the latitude of Las Vegas, Nevada, Wernicke, Brian P. [editor], pp. 391-411.
- Darrow, Arthur, 1972. Origin of the basalts of the Big Pine volcanic field, California, Master's Thesis, UCSB, 61 p.
- Groves, Kristelle, 1996. Geochemical and isotope analysis of Pleistocene basalts from the southern Coso volcanic field, California, Master's Thesis, UNC-Chapel Hill, 84 p.
- LeBas, M.J., LeMaitre, R.W., Streckeisen, A., and Zanettin, B., 1986. A chemical classification of volcanic rocks based on the total alkali silica diagram, J. Petrol. 27:745-750.
- Mullen, E.D., 1983. MnO/ TiO_2/P_2O_5: A minor element discriminant for basaltic rocks of oceanic environments and its implications for petrogenesis, E.P.S.L., 62:53-62.
- Pearce, J.A., Harris, B.W., and Tindle, A.G., 1984. Trace element discrimination diagrams for the tectonic interpretation of granitic rocks, J. Petrol. 25:956-983.
- Ringwood, A.E., 1976. Composition and Petrology of the Earth's mantle, McGraw Hill Book Company, New York, NY, 618 p.
- Sun, S.S and McDonough, W.F., 1989. Chemical and isotopic systematics of oceanic basalts: implications for mantle compositions and processes. *in* Saunders, A.D., and Norry, M.J., Magmatism in the Ocean Basins, Geol. Soc. Spec. Pub. No. 42, pp. 313-345.
- Waits, J.R., 1995. Geochemical and isotope study of peridotite-bearing lavas in eastern California, Master's Thesis, UNC-Chapel Hill, 60 p.
- Wang, K., Plank, T., Walker, J.D., and Smith, E.I., 2002. A mantle melting profile across the Basin and Range, SW USA, Journal of Geophysical Research, pp. ECV 5-1-19.
- Winter, John D., 2001. An Introduction To Igneous and Metamorphic Petrology, Prentice Hall, 699 p.
- Whistler, David P., 1987. Field guide to the geology of Red Rock Canyon and the El Paso Mountains, Mojave Desert, California, NAGT Guidebook, Far Western Section, 16 p.
- Whistler, David P., 1983. Red Rock Canyon; a geologist's classroom, Terra Los Angeles 1982, vol. 21, no. 2, pp. 3-9.

APPENDIX A: TABLE OF MAJOR OXIDES

Sample #	Al2O3	CaO	Fe2O3	K2O	MgO	MnO	Na2O	P2O5	SiO2	TiO2
D2S3	15.5	9.06	12.75	0.44	8.25	0.17	2.48	0.19	49.77	1.38
D3S5DC5	11.96	1.01	2.4	3.32	0.13	0.02	2.9	0.04	78.11	0.12
D3TMI WEST	13.19	1.18	2.02	4.39	0.32	0.02	2.8	0.03	75.96	0.09
WP33S12	14.99	9.61	11.61	0.44	7.77	0.18	2.03	0.21	51.84	1.33
WP49 S1 D2	13.94	9.05	12.14	0.49	8.31	0.13	1.65	0.22	52.53	1.53
D3 TC3	15.87	6.11	10.41	2.65	1.36	0.09	2.9	0.38	58.63	1.6
S22 WP43	14.84	8.89	12.46	0.99	5.39	0.14	1.85	0.22	53.78	1.43
S21 WP42	15.69	9.63	11.84	0.5	3.95	0.18	2.14	0.33	54.4	1.34
S13 WP34	13.04	10.35	11.05	0.56	3.58	0.19	1.02	0.19	58.77	1.24
S16 WP37	13.23	9.01	12.21	0.71	10.14	0.16	0.7	0.2	52.4	1.25
S7 WP25	13.68	9.3	13.54	0.43	9.65	0.14	0.97	0.22	50.52	1.55
WP40 S19	14.88	10.53	13.02	0.49	4.12	0.33	1.82	0.26	53.09	1.46
S26 WP47	14.16	8.45	11.62	0.22	11.63	0.21	1.5	0.19	50.74	1.28
S4 WP52	15.7	8.15	9.76	1.55	4.51	0.19	3.49	0.3	54.93	1.42
S5 WP26	15.73	11.22	9.43	1.24	3.57	0.24	2.29	0.31	54.35	1.63
S1 WP22	15.23	9.5	13.38	0.68	6.62	0.17	1.77	0.25	50.99	1.42
D3 S3 TMI	15.56	6.14	9.14	3.11	0.45	0.08	3.24	0.61	59.55	2.11
D3 S7 TC3	14.43	3.55	5.96	3.54	0.19	0.03	3.28	0.68	67.79	0.55
D3 ST4	14.61	8.68	12.64	0.66	9.81	0.25	2.49	0.21	49.28	1.39
S11 WP32	14.3	9.09	14.07	0.57	6.13	0.15	1.25	0.24	52.65	1.57
D2 S2 WP50	14.99	7.71	10.57	1.4	6.38	0.15	2.83	0.28	54.31	1.39
S3 WP27	16.1	10.07	8.27	0.86	2.57	0.07	2.27	0.4	56.99	2.4
S3 WP24	13.95	8.57	12.08	0.62	9.25	0.18	1.27	0.18	52.61	1.3
S20 WP41	13.92	10.13	10.9	0.67	4.29	0.15	1.49	0.18	56.98	1.29
S17 WP38	15	8.6	12.9	0.86	3.74	0.2	1.72	0.17	55.31	1.52
S14 WP35	12.93	18.72	10.71	0.51	4.39	0.37	1.07	0.2	49.78	1.33
S4 WP25	10.36	36.02	6.79	0.49	2.08	1.14	0.02	0.09	42.29	0.73
D3 S9 TC3	14.99	3.74	5.44	3.03	0.39	0.03	4.13	0.38	66.87	0.99
S10 WP31	14.74	15.05	11.9	0.36	4.37	0.3	1.67	0.22	49.96	1.42
D3 S6 DC5	15	3.56	5.73	3.08	0.32	0.03	4.1	0.3	67.3	0.57
S27 WP48	13.64	8.85	12.58	0.25	11.21	0.25	1.23	0.19	50.48	1.31
WP39 S18	15.59	9.31	12.25	0.49	3.49	0.13	2.21	0.24	54.81	1.48
D3TMI	16.59	5.73	7.95	2.99	0.51	0.06	4.3	0.57	59.26	2.05
S8 WP29	13.75	8.65	11.83	0.47	11.55	0.14	1.36	0.2	50.72	1.32
S24 WP45	15.67	10.71	13.75	0.48	3.09	0.17	2.34	0.54	51.63	1.63
D3 S1 TMI	14.47	1.76	4.18	3.69	0.32	0.02	3.99	0.07	71.27	0.24
DAY2	15.65	9.01	12.18	1.08	7.96	0.17	2.66	0.37	49.56	1.38
S9 WP30	15.2	11.8	13.08	0.33	3.59	0.25	1.79	0.29	52.03	1.64
D3 S13	13.83	8.42	12.17	1.18	10.53	0.15	1.11	0.17	51.23	1.22
D2 S5	15.03	9.44	13.63	0.3	8.21	0.19	2.78	0.19	48.58	1.48
S2 WP23	13.88	9.22	12.61	0.6	9.09	0.25	1.11	0.2	51.77	1.28
S15 WP36	15.01	12.05	12.28	0.44	5.3	0.21	1.91	0.23	51.35	1.23
S23 WP44	14.48	8.2	10.39	0.63	3.49	0.12	1.81	0.2	58.36	1.35
D3 S4 DC5	12.04	1	2.1	3.36	0.08	0.02	2.92	0.09	78.27	0.12

APPENDIX B: TABLE OF TRACE ELEMENTS IN PPM (PARTS PER MILLION)

SAMPLE #	Ba	Ce	Cr	La	Nd	Rb	Sr	Sc	Y	Zr	Sm
D2 S5	56.58	36.54	402.8	13.3	25.83	14.46	423.95	20.36	23.98	110.64	10.16
S4 WP25	94.8	34.44	53.8	5.48	22.1	26.95	324.32	4.2	31.56	96.11	9.2
S27 WP48	339.45	43.64	212.37	12.01	24.2	20.97	425.44	14.19	28.87	122.7	10.45
S15 WP36	329	41.5	189.77	5.71	14.65	22.65	408.81	11.81	28.52	119.5	8.25
S24 WP45	274.83	42.02	225.07	9.84	22.78	14.05	448.74	7.27	28.03	129	8.77
D3 S13	225.79	40.1	260.85	10.15	27.29	44.89	454.78	17.33	35.21	127.51	9.17
WP49 S1 D2	68.22	37.47	271.41	12.6	27.01	26.08	438.97	21.55	33.94	136.42	8.03
S6 WP27	533.87	47.72	554.94	5.95	9.45	43.24	713.45	43.29	57.5	192.37	2.47
S10WP31	164.83	38.48	184.11	0.47	9.07	22.83	431.29	8.24	28.03	120.79	4.61
DAY 2	806.65	55.39	453.29	17.07	32.6	39.1	571.97	17.22	33.8	191.3	10.98
S20 WP41	289.77	41.84	212.46	4.7	13.06	30.47	411.79	0.84	35.51	132.59	5.92
WP40 S19	164.28	39.14	202.38	9.72	22.74	20.24	404.44	20.9	29.7	126.16	7.98
S9 WP30	224.6	40.37	152.97	10.85	21.53	26.95	414.26	12.68	29.37	130.53	8.08
D3 ST4	1008.95	58.87	468.01	13.8	20.24	29.03	584.85	17.76	33	125.7	10.39
S17 WP38	309.2	43	274.25	10.73	19.34	34.09	437.64	15.06	34.63	138.23	10.52
WP39 S18	93.06	36.95	202.81	13.61	15.52	24.66	445.3	1.93	32.68	136.1	8.06
WP33 S12	274.55	41.71	216.33	6.96	17.85	29.82	434.76	2.4	30.48	133.4	7.28
S26 WP47	2052.81	82.68	191.22	13.61	23.78	20.42	455.74	2.4	29.96	129.33	8.48
S2 WP23	339.91	43.36	441.76	13.03	25.66	46.75	480.22	17.87	33.72	116.37	10.27
D2 S2 WP50	643.59	51.33	182.94	13.14	21.01	35.9	659.1	8.96	36.05	187.05	6.63
WP29 S8	57.4	36.26	191.2	7.27	21.49	18.7	392.63	15.17	30.35	125.46	10.15
S11 WP32	304.53	42.24	206.85	15.63	30.34	34.37	391.44	23.6	31.93	126.56	11.31
S5 WP26	4741.73	146	57.96	10.3	14.31	46.97	815.86	8.2	43.1	211.9	2.45
D2 S3	75	37.17	347.98	10.46	18.99	19.71	388.57	5.43	25.97	110.51	9
S14 WP35	203.61	38.29	161.76	2.25	0.91	27.75	356.3	9.22	33.13	112.75	0.69
S22 WP43	710.32	52.47	263.27	9.1	24.23	38.84	441.01	4.78	34.58	134.31	8.64
S21 WP42	1060.93	59.28	188.32	4.59	17.47	24.02	475.73	4.03	32.04	138.43	7.67
S1 WP22	1244.62	64.82	224.95	10.93	24.37	20.22	418.14	16.47	28.65	126.61	8.65
S4 WP52	401.32	46.13	75.6	12.48	11.15	39.52	710.07	-12.42	38.48	208.56	4.13
S16 WP37	217.9	40.23	344.16	6.96	15.28	50.8	428.76	15.17	36.74	121.12	10.34
S3 WP24	794.65	54.75	251.68	7.66	22.43	28.67	426.6	8.57	32.99	129.01	9.35
S7 WP25	291.14	42.49	384.1	13.22	22.08	26.59	443.84	19.17	31.44	125.28	9.09